APPLICATION NOTE

ANP114 | Voltage and Frequency Dependence of Ferroelectric Class 2 Multilayer Ceramic Capacitors

Dr. René Kalbitz

ABSTRACT

After introducing ferroelectricity, a mathematical model for the capacitance-voltage behavior of multilayer ceramic capacitors (MLCCs) is derived from a dipole polarization model. The parameters of the model are reduced to two fitting parameters. The model is tested against measurements from a selection of MLCCs in the Würth Elektronik portfolio to demonstrate practicality. Since the integral of the capacitance-voltage model only contains basic trigonometric mathematical expressions, it can be easily implemented in software requiring functions of charge instead of capacitance, such as Spice simulation software. Furthermore, it is demonstrated that the model can be utilized to describe capacitance spectra of MLCCs at different dc voltages.

01. MOTIVATION AND BACKGROUND

For the design-in process, it has become a common procedure to employ simulation software such as Spice. The developer may load files for multilayer ceramic capacitors (MLCCs) into its software to simulate the influence of the voltage and frequency behavior of the MLCC on its circuit. To make this simulation computationally efficient, it is necessary to implement elegant models for the MLCCs.

In this application note, we briefly review the physical background of the voltage-dependent capacitance of class 2 MLCCs. Furthermore, we describe the mathematical polarization model's development, suitable for simulation software implementation.

An important dielectric property that ceramics can exhibit is ferroelectricity. Ferroelectricity describes the property of a material to form electric dipoles without applying an electric field. Ferroelectricity only occurs in crystals that have a unit cell with no center of symmetry, i.e. non-centrosymmetric shape.[1][2][3][4][5]

In a ferroelectric material, all direct and indirect neighboring cells form the aforementioned dipole, which points in the same direction. The alignment of neighboring dipoles is a result of total energy reduction due to dipole-dipole interactions. The ferroelectric attempts to attain a domain configuration that minimizes the total energy while satisfying both electrostatic and mechanical boundary conditions. [6] In an idealized system, all the dipoles in the crystalline material would collectively point in one direction. Real materials, however, always have minor imperfections that cause the collective orientation of the dipoles to be limited to areas called domains. The size of the domains, crystal configurations at domain boundaries and the orientation of the dipoles within the domains influence the polarizability and, thus, the permittivity of the material [7][8]. This is why MLCCs produced from different raw materials will have different ferroelectric behavior.[1][9][10]

Above the Curie temperature, which is specific for each ferroelectric material, this collective alignment is destroyed. At this phase, the dipoles are randomly aligned and no longer show a domain structure. Under these conditions, the material has paraelectric properties. [11] Ferroelectric materials always show to some degree, paraelectric behavior. Paraelectricity may also be induced by chemical additives, which introduce defective sites and consequently prevent the formation of domains.

A compound used to make MLCCs that has a non-centrosymmetric structure is barium titanate. Figure 1 shows the barium titanate unit cell in which the positively charged titanium ion is shifted slightly (in this representation) upwards with respect to the center. Thus, the unit cell is slightly more positively charged on the “top side” and slightly more negatively charged on the “bottom side”. Since the permanent electric dipole interacts with applied fields, the polarizability and hence the permittivity of such materials is voltage dependent. [7][12]

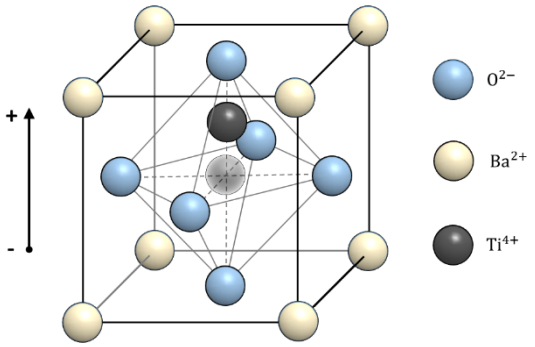

Figure 1: Configuration of the barium titanate unit cell below the Curie temperature. The titanium ion is shifted from the center of the unit cell.

Compared to other materials, ferroelectrics, such as barium titanate, have a high polarizability and, thus, a high relative permittivity. Barium titanate based MLCCs have the benefit of combining low losses with high capacitance and small structural shape. This property makes MLCCs one of the most important passive components for switching converter circuits and filter applications. [10]

The trade-off of the large capacitance in ferroelectric class 2 MLCCs is the above-mentioned voltage dependence that leads to a disadvantageous decrease of capacitance with increasing DC voltage. In the further course of this note, we will first explain the polarization processes and secondly develop a model, designed to describe the voltage-dependent capacitance.

02. INTERPRETATION OF CAPACITANCE-VOLTAGE MEASUREMENTS

Ferroelectric polarization is well studied and shall be reviewed briefly. [1][9][13] The polarization behavior of ferroelectric materials depends on the actual state of polarization, as shall be discussed with the capacitance-voltage and polarization-voltage graphs of a 10 µF MLCC (class 2), shown in Figure 2.

During the measurement, a sinus probing waveform of frequency f is applied to measure the capacitance of the capacitor. The ac probing waveform has a fixed amplitude throughout the measurement and induces a periodical change of voltage dV. On the sinus signal, a dc voltage is superimposed, allowing the reorientation of the domain polarization.

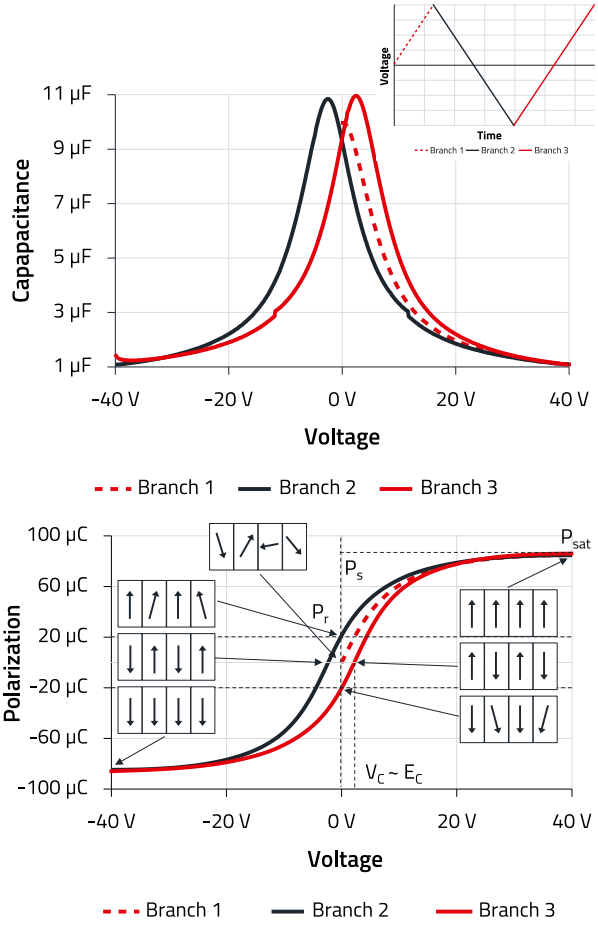

Figure 2: TOP: Measured capacitance-voltage characteristics of 10µF MLCC, for a voltage cycle, shown in the inset graph. BOTTOM: Polarization-voltage characteristics with corresponding schematic depiction of dipole orientation.

Branch 1:

The capacitor, with randomly oriented domain polarizations, is subjected to the test signal. With the increase of dc voltage, the dipoles eventually become aligned, leading to increased polarization (Figure 2). Saturation polarization is reached when all dipoles ideally point in the direction of the external electric field. As the voltage increases, the dipoles become aligned and the dipole movement becomes more restricted, which leads to a reduced charge change of charge dq. Hence, the capacitance C = dq/dV decreases with increasing dc voltage.

When the applied external field E, which is proportional to the applied voltage, has aligned the majority of the domains, the dipoles remain in this position even without the external field. The collective alignment creates an internal stabilizing coercive field, E_c. As the applied electric field increases, the overall polarization increases due to other polarization effects such as electronic, ionic and dipolar types.

The polarization at maximum voltage is referred to as saturation polarization P_{sat}. In principle, the spontaneous polarization P_s is equal to the saturation polarization of the electric displacement extrapolated to zero field strength.

Branch 2:

As the voltage, and with that, the external field, is reversed from positive to negative, the dipoles relax slightly but remain in their overall polarization direction due to the internal coercive field, E_c. The polarization state at zero volts is referred to as remanent polarization P_r.

Any reversed external electric field will have to exceed E_c in order to reorient all domains into the opposite direction. At the position of E_c the strain on the dipoles is least, thus the materials permittivity (susceptibility) is largest and the capacitance shows a local maximum. With the increase of polarization into the opposite direction, the capacitance decreases to the same value as for positive voltages.

Branch 3:

If the voltage is driven from negative to positive, the dipoles reorient again when the externally applied field exceeds the coercive field. This, again, leads to a peak at the capacitance at positive voltages. The process is similar to the one described before. Branch 3 is similar to branch 2, except it is shifted along the x-axis toward positive voltages.

The above-described hysteresis requires the distinction between the polarizations for voltage sweeps from positive to negative and vice versa. Therefore, in the further course, $P^+(E)$ denotes the polarization (branch 2) for voltage sweeps from positive to negative and $P^-(E)$ (branch 3) the polarization for voltage weeps from negative to positive voltages.

Hence, any increase in dc voltage leads to a decrease in capacitance. However, the capacitance is further decreased with an increasing application time of dc voltage. That further decrease is related to the retarded movement of the domain walls, caused by domain wall pinning. [14][15][16][17] Domain wall motion takes place on a longer timescale than the initial reorientation of dipoles, which occurs on a sub-second timescale. [19] Domain wall movement generally leads to an additional gradual decrease of the capacitance of up to 20 %, which can take place over a period of up to 1000 hours. [14][15]

This long-term effect should only be mentioned at this point for the sake of completeness and to hint at the complexity of dc measurements. However, for the sake of clarity, the note will keep the focus on the dc dependency.

Besides the domain wall movement, a field-induced phase transition may occur on some pristine barium titanate compounds [20][21]. During this process, the unit cell undergoes a structural change, resulting in the formation of the permanent dipole. This kind of phase transition causes a peak in the capacitance-voltage measurements even during the first sweep (Branch 1), which is similar to the one exhibited during the reorientation of the dipoles (in branch 2 and branch 3). Hence, the origin of the peak is not the reorientation of the dipoles but the reconfiguration of the unit cell in at least some fractions of the material. Such a behavior is not visible in this measurement shown here but may be in others.

03. MATHEMATICAL MODEL OF FERROELECTRIC POLARIZATION

The following section introduces a semi-phenomenological polarization model for capacitance-voltage measurements. Corresponding mathematical details are found in section 8. [13] The parameters of the model are related to measurable and physically meaningful quantities such as remanent and spontaneous polarization.

The physics of ferroelectric and paraelectric materials are well discussed in scientific literature, which provides a solid basis for the development of a model suitable for technical applications such as electrical circuit simulation. [1][13][22][23]

A model that is based on an ideal polarization behavior is:[13]

$$C(V) = (a - C_s)\,\mathrm{sech}^2\left(\frac{V - V_C}{b}\right)^{\square} + C_s \qquad (1)$$

with C_s as the linear contribution to the capacitance (voltage-independent pure capacitive part), V_C as the coercive voltage ($V_C \propto E_c$), a as the factor proportional to saturation polarization and b as the factor related to the width of the bell-shaped curve. As discussed in section 8, this model depends on ideal assumptions such as complete polarization, a homogenous electric field and homogeneous dipole distribution based on homogeneous material composition. The advantage of this model is that a, b, C_s and V_C can be retrieved directly from the measured data, i.e. no fitting is required. C_s is the capacitance at the maximum voltage, (a-C_s) is the height of the peak (max. of C(V)), V_C is the position of the peak and b can be calculated from C(V) with the inverse of the hyperbolic secant (see section 8).

Whether or not the polarization model originally published by Miller et al. [13] is based on first principles is of no importance at this point. What is relevant is the numerical simplicity, since

the parameters can be clearly related to characteristic features of the measured data. Consequently, this leads to a situation where the set of parameters is relatively small and easily retrievable from the measurement.

Figure 3 shows a C-V measurement of a 10 µF class 2 MLCC, which was measured with consecutive voltage sweeps, along with a fitted equation (1). Although the fit is not perfect, especially the features between -10 V and +10 V are well described by the model. The two visible peaks of the positive and negative branch occur, if the external field reaches the coercive field strength and cause a reversal of the dipole orientation. At this moment, the dipoles have large mobility, i.e. the change of charge is large. Thus the capacitance has a local maximum at this position.[1]

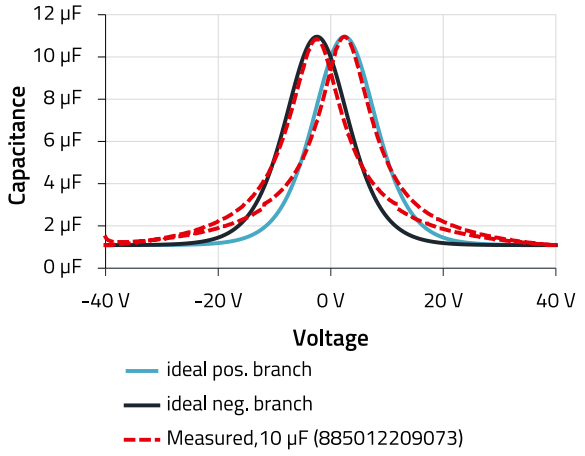

Figure 3: Measured capacitance-voltage characteristic of 10 µF MLCC with the corresponding fit of equ. (1). Numerical fit-parameters: a = 10.85, b = 7.5, C_s = 1.09, V_C = 2.5.

When used on a measurement of a commercially available MLCC, as in Figure 3, the above function C(V) does model the overall behavior. However, if the voltage exceeds |±10 V| the measured capacitance is larger than calculated by the model. The reason for this discrepancy could be the inhomogeneous electric field, caused by the interdigitated electrode geometry of the MLCC, inhomogeneous material composition as well as retarded switching behavior caused by domain wall pinning/switching.[14, 15] Hence, the MLCC consists of fractions of material, which show different voltage behavior or ferroelectric behavior.

Theoretically, it would be possible to model such MLCCs as a superposition of equation (1).

$$C_P = \sum_i a_i \operatorname{sech}^2\left(\frac{V - V_{Ci}}{b_i}\right), \qquad (2)$$

where each aforementioned material fraction, indicated by i, is represented by a set of parameters a_i, V_{Ci} and b_i. equation (2) is a physically valid approach, however, makes a fitting elaborate and thus impractical for an extensive portfolio of MLCCs. Conversely, it would be time-consuming to implement this function in the simulation file and execute it in the simulation software.

In practice, for the modeling of most measurements, it is sufficient to use three summands

$$C_P = \left(\frac{a^*}{a_0}\right) \left[\operatorname{sech}^2\left(10\frac{V - V_C}{7 \cdot b}\right) + \frac{b}{30}\operatorname{sech}^2\left(\frac{V - \frac{V_{max}}{8} + V_c}{2 \cdot b}\right) + + \frac{b}{30}\operatorname{sech}^2\left(\frac{V + \frac{V_{max}}{8} - V_c}{2 \cdot b}\right)\right] - C_s \cdot \frac{h}{10} \qquad (3)$$

with V_{max} as the maximum voltage, h as the non-saturated correction factor for C_s, $a^* = C_s \cdot (h/10-1)+a$ as effective peak height and with

$$a_0 = 1 + 2\frac{b}{30}\operatorname{sech}^2\left(\frac{\frac{V_{max}}{8}}{2 \cdot b}\right), \qquad (4)$$

as a normalization factor, which corrects for the additional offset due to the three terms. Hence, C_P consists of a main contribution (first sech^2 term) and two broader secondary contributions (second and third sech^2 term), positioned at fixed distances to the left and right of the main contribution, as shown exemplarily for branch 3 in Figure 4. The offset $-C_s \cdot h/10$ corrects for the pure capacitive contribution. Since in most cases the voltage is insufficient for a complete polarization event, the factor h/10 has been introduced to account for the non-saturated dipole contribution.

The specific choice of parameters/factors concerning the voltage shift, the width and height of the secondary contributions was found to give good results for a range of measurements. The factors can still be differently adjusted, if necessary.

To demonstrate the practicality of the model, as given in equ. (3), a selection of fit results is given in Table 2 (Section 8, Appendix). The fits yield root mean square relative error values of around 1% or below, which is still well below the capacitance production tolerance of 10%.

Equation (3) has the benefit of reducing the fitting parameters down to b and h. The other parameters can be inferred directly from the capacitance-voltage measurement. Parameter V_{max} is the maximal voltage applied during the sweep voltage with $C_s = C(V_{max})$. Parameters a and V_c are the value of the local maximum and its position, respectively. In

the case of pristine preheated samples with little or no spontaneous polarization present, it is possible to set $V_c = 0$.

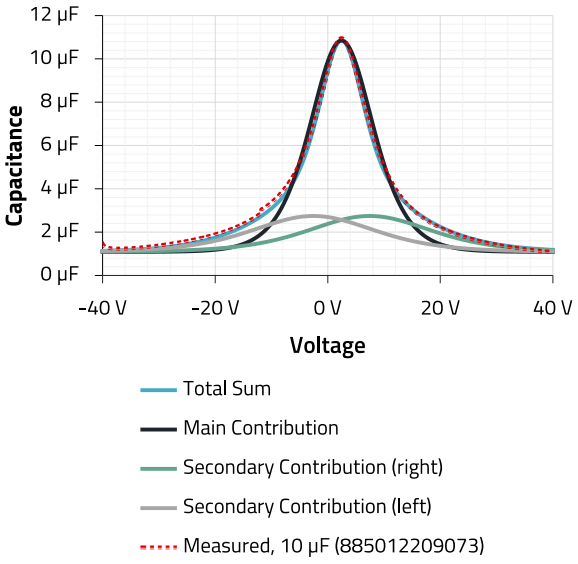

Figure 4: Measured capacitance-voltage characteristic of 10 µF MLCC with the corresponding fit of equ. (5) and its corresponding contribution, i.e. summands. Dimensionless numerical fit-parameters: a = 10.85, b = 7.3, V_{max} = 4.0, C_s = 1.09, V_C = 2.45 and h = 0.01.

$$C(V) = C_P + C_s \quad (5)$$

Equation **Error! Reference source not found.** may be used to fit the capacitive-voltage behavior of a large portfolio of MLCCs. Table 2 in section 8 lists the fitting parameters along with the root mean square relative error for a selection of MLCC.

Please note, that an additional even more simplified mathematical approach for C(V), equivalent to the one presented here, is given in Section 8. For sake of clarity, it is not included in the following discussion.

The implementation of mathematical models in some simulation software, such as LTspice, requires a function of polarization, i.e. charge equation (see Section 8)

$$\Delta q = \int C(V)\, dV \quad (6)$$

Since the integral of $Sech^2$-functions yields Tanh-functions, which are available in most script languages, the implementation of the fitted equation (5) into simulation software is straightforward.

04. EXPERIMENTAL DETAILS

Before the measurements, all capacitors have been annealed for at least 1 h at 150°C. The subsequent cool-down time was 24 h. All measurements were performed at room temperature.

For the C-f measurements, the impedance analyzer E4990A from Keysight was used in conjunction with the test fixture 16034E. The ac probing voltage amplitude of the impedance analyzer, superimposed to the dc voltage, was V_{rms} = 0.250 V. The pre-conditioning time for the parametric dc voltage, applied during the frequency sweep, was 20 h.

For the hysteresis and time-dependent measurement, the LCR meter E4980A from Keysight was used in conjunction with the test fixture 16034G. The ac probing voltage amplitude of the LCR meter was V_{rms} = 1 V and the corresponding probing frequency was 1 khz.

05. IMPLEMENTATION: INITIAL STATE OF POLARIZATION AND MEASUREMENT CONDITION

In addition to the measurement time, it is required to define the initial state of polarization. As explained above, the voltage dependence of the capacitance depends on the initial state of polarization, which is not known in the application case.

For the operational data acquisition, the fitting data was obtained from pristine MLCC batches, which were preheated above the Curie temperature. Hence, for the model in equ. (5) the voltage shift is $V_C = 0$.

The initial state may not be easily defined in composites of barium titanate, since, depending on the composition, some may exhibit a field-induced phase transition. As explained in section 2, such a process results in a peak in the capacitance-voltage characteristic even during the first sweep (after the sample was annealed).

Also, the domain wall movement may cause slight variations in the capacitance-voltage characteristics depending on the scanning speed. In practice, this is a phenomenon that is difficult to control.

Hence, capacitance-voltage scans of the two MLCCs with identical part numbers can deviate from one another depending on the exact measurement conditions and slight differences in their chemical and structural composition.

06. IMPLEMENTATION: FREQUENCY AND VOLTAGE-DEPENDENT MODEL

In the previous sections, we mainly discussed the voltage dependence of the model. However, for applications such as filters and converters, it will be important that the model

describes the frequency behavior correctly as well. Typically, the impedance of capacitors are modelled with

$$Z(\omega,V) = R_{ESR} + \left(i\cdot\omega\cdot C(V)+R_{ins}^{-1}\right)^{-1} + i\cdot\omega\cdot L \qquad (7)$$

with $\omega = 2\ \pi\ f$ as angular frequency, $i=\sqrt{(-1)}$ as imaginary unit, R_{ESR} as equivalent series resistance, R_{ins} as insulation resistance, L as parasitic inductance and C(V) as the voltage-dependent capacitance, given by equ. (5). Each capacitor is consequently modeled by an individual set of parameters: a, b, h, C_s, V_{max}, R_{ESR}, R_{ins} as well as L.

The impedance model $Z(\omega,V)$ (equ. (7)) assumes the same frequency behavior for C_s and C_p, which might not be the case in reality. The hysteresis behavior depends on the scanning frequency, i.e. the voltage rise time, of the dc voltage. [19] That implies the model is most accurate when the ac voltage is about or smaller than the coercive voltage V_c. Thus, we estimate that the model is accurate, if the ac voltage amplitude is below 10% of the rated voltage.

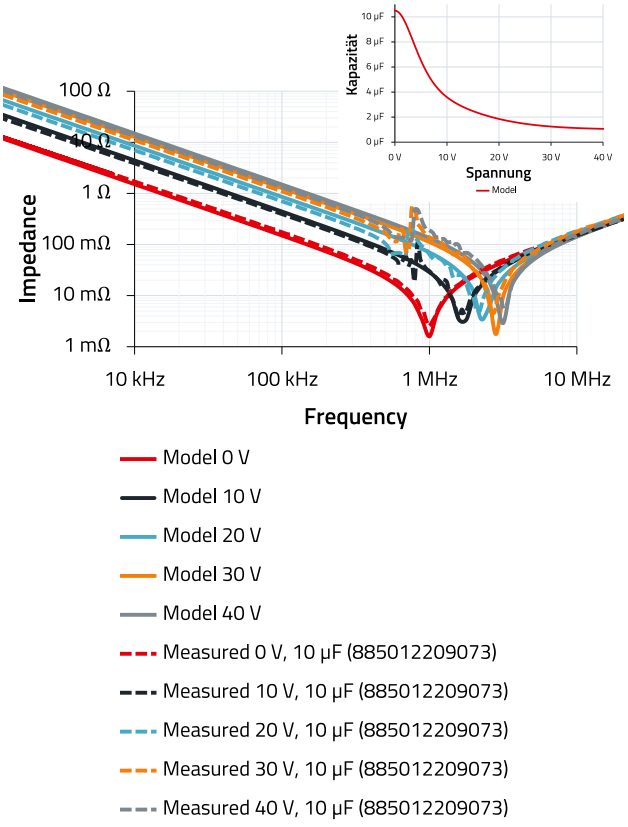

Figure 5: Measured and calculated impedance spectra for different dc-voltages. Inset graph shows corresponding C-V function.

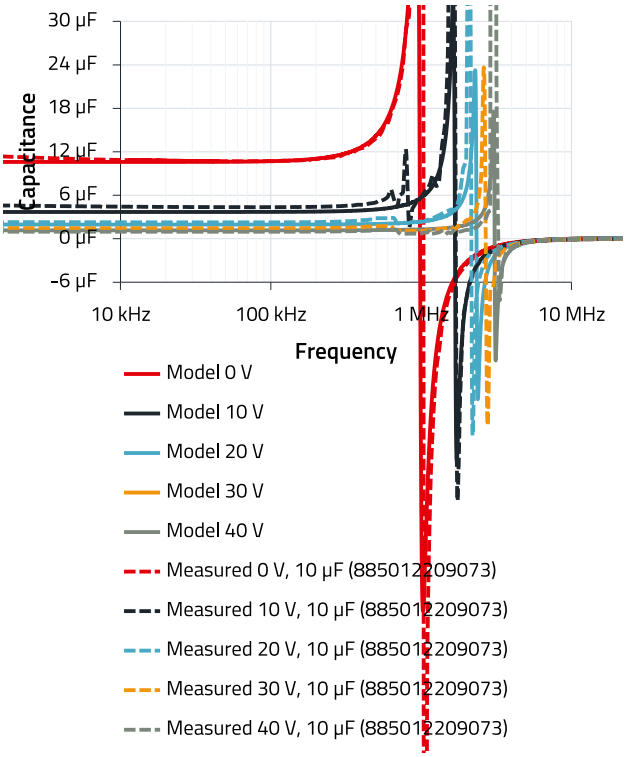

Figure 6: Measured and calculated capacitance spectra for different dc-voltages.

Figure 5 and Figure 6 show a good agreement of the calculated graphs with the measured impedance and capacitance spectra, respectively, for different voltages. The spectra were taken after a pre-conditioning time of 40 h to include the effect of domain wall switching. The inset graph in Figure 5 shows the corresponding capacitance-voltage function, as obtained with the parameters, given in Table 1.

Parameter	Value
a	$1 \cdot 10^{-5}$
b	7.3
h	0
C_s	$1 \cdot 10^{-6}$
V_{max}	40
V_c	0
R_{ESR}	$1.5 \cdot 10^{-3}$
R_{ins}	$5 \cdot 10^{6}$
L	$2.5 \cdot 10^{-9}$

Table 1: Fitting parameters with units as used for graphs in Figure 5 and Figure 6.

In this example, the deviations between the theoretical and measured spectra are caused by the slight deficiencies the capacitance model may have at intermediate values. Considering the difficulties in precisely measuring the long-

term dc effect, we assess the accuracy as satisfactory for practical application. The cause of the small spikes (noise) just below 10^6 Hz in the graphs measured with applied dc-voltage could not be clearly identified. The fact that they are in different graphs roughly in the same frequency range could indicate a setup-related measurement artifact.

Due to the manifold of influencing parameters on ferroelectricity such as temperature, domain wall switching dynamics, voltage aging and slight variations of chemical compositions of raw materials, the exact modeling of C-V characteristics is a challenge. Because of the complexity of the issue, it remains necessary that electrical engineers complement model-based data with application-based tests and measurements.

07. CONCLUSION

After a short introduction to ferroelectricity, we have developed a semi-phenomenological model based on a theory for ferroelectric polarization developed by Miller.[13] The model given in equation (3), has the advantage of reducing the fitting parameters down to b and h. The other parameters a, C_s, V_{max}, and V_c can be read directly from the capacitance-voltage measurement. In the case of pristine preheated samples, it is possible to assume $V_c = 0$.

We have demonstrated using the example of a 10 µF class 2 MLCC that the model provides a qualitatively satisfactory description of the C-V behavior and the corresponding spectra. It is based on the main assumptions that the MLCC:

is in a random polarization state, i.e. was previously annealed above the Curie temperature and is subjected to ac voltages, which are about 10% of the rated voltage.

Overall, the calculated spectra are in good agreement with the measured spectra.

Acknowledgment

Special thanks to the technical experts Eric Fischer as well as Jon Izkue-Rodriguez at Würth Elektronik, who provided measurements as well as technical support.

A Appendix

A.1 Alternative Mathematical Model

As an alternative approach, we propose the modified equation

$$C_P \cong a \cdot \operatorname{sech}^c\left(\frac{V - V_C}{b}\right) \quad (8)$$

which allows the change of the slope gradient by the exponent c. Although c is not directly related to a physical quantity, its introduction significantly simplifies the model.

Thus, the measured capacitance can be fitted with

$$C(V) = (a - C_s) \cdot \operatorname{sech}^c\left(\frac{V - V_C}{b}\right) + C_s \quad (9)$$

With this set of five parameters a,b,c,V_C and C_s it is possible to model the measured voltage-dependent capacitance with sufficient accuracy as demonstrated in Figure 7. The first term of equ. (9)

$$C_p = (a - C_s) \cdot \operatorname{sech}\left(\frac{V - V_C}{b}\right) \quad (10)$$

models the voltage-dependent contribution of polarization to the capacitance and C_s, the voltage-independent pure capacitive part.

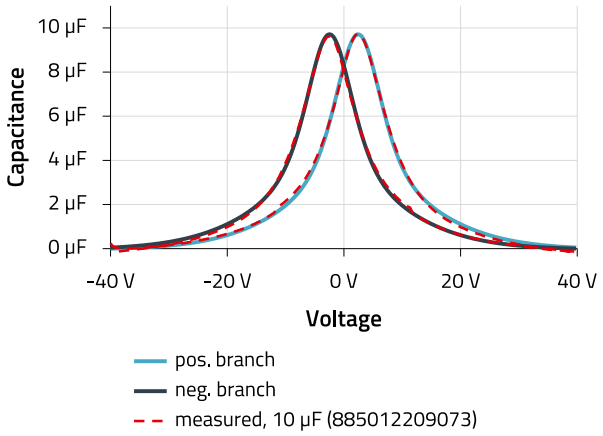

Figure 7: Measured capacitance-voltage characteristic of 10 µF MLCC with the corresponding fit of equ. (9). Dimensionless numerical fit-parameters: a=10.85, b=1.3, c=0.17, C_s=1.09, V_C=2.5.

Although the numeric and symbolic integration for equ. (9) is always possible, the symbolic integration may involve hypergeometric functions, which may not be supported in the simulation software. This can be avoided for c=1 and c=2 as shown below. Under these conditions, the model of the capacitance and its charge, Δq, as calculated with equ.(6), can be expressed with trigonometric functions. Trigonometric functions are usually implemented in the script language of the simulation tools, such as LTspice.

The corresponding charge equation is

$$\Delta q(V) = 2b\,(a - C_s)\arctan\left[\tanh\left(\frac{V}{2b}\right)\right] + C_s V \quad (11)$$

Polarization Contribution to Capacitance

The relation between polarization and capacitance is derived from the definition of capacitance C = dq/dV, the definition of electric current I = (dq)/dt and charge conservation

$$I = A\frac{dP}{dt} + C_s\frac{dV}{dt} + I_0(V) \quad (12)$$

with A as the effective area of the capacitor, C_s as the pure capacitive contribution and $I_0(V)$ as other voltage-dependent contributions, such as ohmic currents, e.g. $I_0(V) = V/R$. Hence, the measured capacitance becomes

$$C = \left(A\frac{dP}{dt} + C_s\frac{dV}{dt} + I_0(V)\right)\frac{dt}{dV} \quad (13)$$

$$C = A\frac{dP}{dV} + C_s + I_0(V)\frac{dt}{dV}$$

$$C = C_p + C_s + C_V^0 \quad (14)$$

with C_p as the dipole polarization contribution to the capacitance, C_s as the pure capacitive contribution and C_V^0 as further capacitive contributions, such as leakage currents or possible electrochemical effects.

For the sake of simplicity, C_V^0 may be neglected in all further considerations. A practical approach, capable of modeling commercial ceramic capacitors in good agreement with the measurements is

$$C = C_p + C_s. \quad (15)$$

The ideal field-depended polarization can be modelled with

$$P^+(E) = P_s \tanh\left(\frac{E - E_C}{2\delta}\right) \quad (16)$$

with

$$\delta = E_C\left[\frac{1 + \frac{P_r}{P_s}}{1 - \frac{P_r}{P_s}}\right]^{-1}$$

where P_r and P_s denotes the remanent and spontaneous polarizations, respectiely. [13]

The negative-going branch of the saturated hysteresis loop $P^-(E)$ is shifted along the x-axes and given by $P^-(E) = P^+(-E)$. For the sake of simplicity we may skip the index in the further discussion. The electric field E = V/d is proportional to the applied voltage, with d as the effective capacitor thickness.

With equ (15) and (16) the ideal capacitance of ferroelectric material can be calculated as

$$C(V) = A\,\frac{P_s}{2\,\delta\,d}\,\mathrm{sech}^2\left(\frac{V - V_c}{2\,\delta\,d}\right)^{\square} + C_s \qquad (17)$$

where the first term models the contribution of polarization to the capacitance and the second term constitutes the purely linear capacitive contribution. This expression does not yet contain any explicit dependence on the frequency. It provides a model for the voltage dependence with frequency as a constant parameter. The main frequency-dependent quantities are $C_s(f)$ and $P_s(f)$. This model does not yet describe the frequency dependence of C_p, which might differ from C_s.

For the fitting of measured C(V) data, equ. (17) can be rewritten and substituted with fitting factors a,b,V_C and C_s:

$$C(V) = a\,\mathrm{sech}^2\left(\frac{V - V_C}{b}\right)^{\square} + C_s \qquad (18)$$

Note that b is related to C(V) with

$$b = \frac{V - V_c}{\mathrm{arsech}(\sqrt{C(V) - C_s})} \qquad (19)$$

Integration of Hyperbolic Secant and C(V)

Generally, the expression of polarization $\Delta q/A$ or change of charge Δq is obtained by integration of C(V)

$$\int (C_p + C_s)dV = \int dq_p + \int dq_s = \Delta q_p + \Delta q_s \qquad (20)$$

Example of calculation for c=1:

$$C=(a-C_s)\cdot\mathrm{sech}\left(\frac{V}{b}\right)^{\square} + C_s \qquad (21)$$

$$C_p(V)=(a-C_s)\cdot\mathrm{sech}\left(\frac{V}{b}\right)^{\square}$$

$$\Delta q_p = \int C_p dV = 2c(a-C_s)\arctan\left[\tanh\left(\frac{V}{2\,b}\right)\right]$$

$$\Delta q_s = \int C_s dV = C_s V$$

$$\Delta q = \Delta q_p + \Delta q_s = 2c(a-C_s)\cdot\arctan\left[\tanh\left(\frac{V}{2\,b}\right)\right] + C_s V \qquad (22)$$

Example of calculation for $c = 2$:

$$C=(a-C_s)\cdot\mathrm{sech}^2\left(\frac{V}{b}\right)^{\square} + C_s \qquad (23)$$

$$C_p(V)=(a-C_s)\cdot\mathrm{sech}^2\left(\frac{V}{b}\right)^{\square}$$

$$\Delta q_p = \int C_p dV = b(a-C_s)\tanh\left(\frac{V}{b}\right)$$

$$\Delta q_s = \int C_s dV = C_s V$$

$$\Delta q = \Delta q_p + \Delta q_s = b(a-C_s)\cdot\tanh\left(\frac{V}{b}\right) + C_s V \qquad (24)$$

Example of calculation for C_P in equation (3):

$$C_p = \left(\frac{a^*}{a_0}\right)\left[\mathrm{sech}^2\left(10\,\frac{V-V_C}{7\cdot b}\right) + \frac{b}{30}\,\mathrm{sech}^2\left(\frac{V-\frac{V_{max}}{8}+V_c}{2\cdot b}\right) + \frac{b}{30}\,\mathrm{sech}^2\left(\frac{V+\frac{V_{max}}{8}-V_c}{2\cdot b}\right)\right] - C_s\cdot\frac{h}{10}$$

$$\begin{aligned} q_p = \int C_p dV = {} & \left(\frac{a^*}{a_0}\right)\cdot\frac{7\cdot b}{10} \\ & \cdot\tanh\left(\frac{V-V_C-\frac{V_{max}}{8}}{7b}\right) \\ & + \left(\frac{a^*}{a_0}\right)\cdot\frac{2\cdot b^2}{30} \\ & \cdot\tanh\left(\frac{V-V_C-\frac{V_{max}}{8}}{2b}\right) \\ & + \left(\frac{a^*}{a_0}\right)\cdot\frac{2\cdot b^2}{30} \\ & \cdot\tanh\left(\frac{V-V_C+\frac{V_{max}}{8}}{2b}\right) - C_s \\ & \cdot\frac{h}{10}\cdot V \end{aligned} \qquad (25)$$

Fitting Results

The results in Table 2 are based on a fit of equ. (3) on data given in the REDEXPERT Design Platform. The fits were performed by utilizing the FindFit function in Wolfram Mathematica. The base units for the capacitance and voltage were nF and V, respectively. All fitting errors were around or below 1%, which is well below the ±10% capacitance tolerances of the MLCCs. The measurements were performed and provided by courtesy of Jon-Izkue-Rodrigues and Eric Fischer.

Articlenumber	$a \cdot 10^{-3}$	$a^* \cdot 10^{-4}$	h	b	$C_s \cdot 10^{-4}$	V_{max}	Root Mean Square Relative Error, RMSRE
885012109004	100000	9189.93	8.02	6.08	4092.09	6.30	0.0070
885012109011	47000	4507.34	8.06	8.41	994.57	16.00	0.0090
885012109010	22000	4395.28	29.51	25.43	1125.23	16.00	0.0142
885012108012	47000	4355.12	6.58	5.66	1007.52	10.00	0.0087
885012108011	22000	2172.04	9.47	6.75	528.39	10.00	0.0194
885012108003	22000	2127.95	9.34	7.42	1098.02	6.30	0.0129
885012108018	22000	2123.46	7.84	7.44	354.40	16.00	0.0130
885012107011	22000	2035.90	6.05	5.21	415.73	10.00	0.0117
885012107005	22000	1916.61	5.00	4.01	566.77	6.30	0.0151
885012108001	4700	1634.89	40.00	26.33	388.30	6.30	0.0113
885012208017	4700	1589.92	40.00	35.39	373.31	10.00	0.0155
885012207024	2200	690.93	40.00	29.17	156.98	10.00	0.0164
885012108009	6800	663.08	9.45	9.99	307.22	10.00	0.0038
885012108008	4700	604.22	14.57	15.94	293.93	10.00	0.0096
885012108014	2200	590.17	40.00	31.68	123.39	16.00	0.0179
885012208038	2200	580.55	40.00	30.81	120.18	16.00	0.0167
885012207021	680	244.03	40.00	43.37	58.68	10.00	0.0089
885012106018	2200	205.86	6.87	7.86	45.18	16.00	0.0035
885012106008	470	149.44	40.00	29.66	34.15	10.00	0.0086

*Table 2: Fitting results for selected **MLCCs** from Würth Elektronik ranging from 100µF to 470nF with equations (3)and (5). Capacitance-voltage measurements used for the fitting are presented in the **REDEXPERT** Design Platform. The units of the measured capacitance-voltage data were in pF and volts. The coercive voltage was set to V_c=0. Only the parameters h and b have been fitted with a minimization algorithm of Wolfram Mathematica. C_s. V_{max} and a were directly taken from the measured capacitance-voltage values C(V). The parameter C_s relates to the maximum voltage with V_{max} by C_s=C(V_{max}). The parameter a is the actual measured capacitance value in units of nF at V = 0.*

A.2 References

[1] R. C. Buchanan (ed.). Ceramic Materials for Electronics. Third Edition. CRC Press Taylor & Francis Ltd (2018)

[2] M.J. Pan. A Brief Introduction to Ceramic Capacitors. DEIS Feature Article. IEEE Electrical Insulation Magazine. pp. 44-50 (2010)

[3] A. von Hippel. Ferroelectricity. Domain Structure. and Phase Transitions of Barium Titanate. Reviews of Modern Physics. 22. 221-237 (1950)

[4] Haertling. Ferroelectric Ceramics: History and Technology. Journal of American Ceramic Society. 82. 797-818 (1999)

[5] P. Popper. Ceramic Dielectrics and their Applications to Capacitors for Use in Electronic Equipment. Proceedings of the IEE - Part IIA: Insulating Materials. 100. 229-238 (1953)

[6] B. G. Potter Jr. et al. Monte Carlo simulation of ferroelectric domain structure: Electrostatic and elastic strain energy contributions. AIP Conference Proceedings 535. 173 (2000)

[7] Uchino. Ceramic Actuators: Principles and Applications. MRS Bulletin. 80. 42-48 (1993)

[8] G. Arlt et al.. Domain configuration and equilibrium size of domains in BaTiO3 ceramics. 51. 4956-4960 (1980)

[9] W. Geng et al.. Temperature dependence of ferroelectric property and leakage mechanism in Mn-doped $Pb(Zr_{0.3}\ Ti_{0.7})O_3$ films. Ceramics International. 47:17. 24047-24052 (2021)

[10] K. Hong et al.. Perspective and challenges in multilayer ceramic capacitors for next generation electronics. J. Mater. Chem. C. 7. 9782-9802 (2019)

[11] Mahesh Peddigari et al.. Linear and Nonlinear Dielectric Ceramics for High-Power Energy Storage Capacitor Applications. Journal of the Korean Ceramic Society 56:1 (2018)

[12] W.S. Ohm. Control of Electromechanical Properties of Multilayer Ceramic Capacitors for Vibration Reduction. Journal of the American Ceramic Society. 1001. 1982-1990 (2018)

[13] S.L. Miller et al.. Modeling ferroelectric capacitor switching with asymmetric nonperiodic input signals and arbitrary initial conditions. Journal of Applied Physics. 70:2849-2860 (1991)

[14] T. Tsurumi et al.. Mechanism of Capacitance Aging under DC Electric Fields in Multilayer Ceramic Capacitors with X7R Characteristics. Japanese Journal of Applied Physics. 44. 6989 (2005)

[15] T. Tsurumi et al.. Mechanism of capacitance aging under DC-bias field in X7R-MLCCs. J Electroceram 21. 17–21 (2008)

[16] T. Teranishi et al.. Domain contribution to the aging characteristics in $BaTiO_3$ ceramics. Jpn. J. Appl. Phys.. 58:SLLC03 (2019)

[17] J. Guyonnet. Ferroelectric Domain Walls - Statics. Dynamics. and Functionalities Revealed by Atomic Force Microscopy. Springer Cham. Springer Theses (2014)

[18] S. Wada et al.. DomainWall Engineering in Barium Titanate Single Crystals for Enhanced Piezoelectric Properties. Ferroelectrics. 334. 17–27 (2006)

[19] Y. Li et al.. Switching dynamics of ferroelectric HfO_2 -ZrO_2 with various ZrO_2 contents. Appl. Phys. Lett. 114:14. 142902 (2019)

[20] J. E. Daniels et al.. Electric-field-induced phase transformation at a lead-free morphotropic phase boundary: Case study in a 93 % ($Bi_{0.5}\ Na_{0.5}$) TiO_3 – 7 % $BaTiO_3$ piezoelectric ceramic. J. Appl. Phys. 95. 032904 (2009)

[21] T Iamsasri et al.. Time and frequency-dependence of the electric field-induced phase transition in $BaTiO_3$ -$BiZn_{1/2}\ Ti_{1/2}\ O_3$. J. Appl. Phys. 122. 064104 (2017)

[22] K. M. Johnson. Variation of Dielectric Constant with Voltage in Ferroelectrics and Its Application to Parametric Devices. Journal of Applied Physics. 33:9. 2826-2831 (1962)

[23] Y. Zhang. Electric Field-Dependent Dielectric Properties and High Tunability of Porous $Ba_{0.5}\ Sr_{0.5}\ TiO_3$ Ceramics. J. Am. Ceram. Soc.. 90:4. 1327–1330 (2007)

IMPORTANT NOTICE

The Application Note is based on our knowledge and experience of typical requirements concerning these areas. It serves as general guidance and should not be construed as a commitment for the suitability for customer applications by Würth Elektronik eiSos GmbH & Co. KG. The information in the Application Note is subject to change without notice. This document and parts thereof must not be reproduced or copied without written permission. and contents thereof must not be imparted to a third party nor be used for any unauthorized purpose.

Würth Elektronik eiSos GmbH & Co. KG and its subsidiaries and affiliates (WE) are not liable for application assistance of any kind. Customers may use WE's assistance and product recommendations for their applications and design. The responsibility for the applicability and use of WE Products in a particular customer design is always solely within the authority of the customer. Due to this fact it is up to the customer to evaluate and investigate. where appropriate. and decide whether the device with the specific product characteristics described in the product specification is valid and suitable for the respective customer application or not.

The technical specifications are stated in the current data sheet of the products. Therefore the customers shall use the data sheets and are cautioned to verify that data sheets are current. The current data sheets can be downloaded at www.we-online.com. Customers shall strictly observe any product-specific notes. cautions and warnings. WE reserves the right to make corrections. modifications. enhancements. improvements. and other changes to its products and services.

WE DOES NOT WARRANT OR REPRESENT THAT ANY LICENSE. EITHER EXPRESS OR IMPLIED. IS GRANTED UNDER ANY PATENT RIGHT. COPYRIGHT. MASK WORK RIGHT. OR OTHER INTELLECTUAL PROPERTY RIGHT RELATING TO ANY COMBINATION. MACHINE. OR PROCESS IN WHICH WE PRODUCTS OR SERVICES ARE USED. INFORMATION PUBLISHED BY WE REGARDING THIRD-PARTY PRODUCTS OR SERVICES DOES NOT CONSTITUTE A LICENSE FROM WE TO USE SUCH PRODUCTS OR SERVICES OR A WARRANTY OR ENDORSEMENT THEREOF.

WE products are not authorized for use in safety-critical applications. or where a failure of the product is reasonably expected to cause severe personal injury or death. Moreover. WE products are neither designed nor intended for use in areas such as military. aerospace. aviation. nuclear control. submarine. transportation (automotive control. train control. ship control). transportation signal. disaster prevention. medical. public information network etc. Customers shall inform WE about the intent of such usage before design-in stage. In certain customer applications requiring a very high level of safety and in which the malfunction or failure of an electronic component could endanger human life or health. customers must ensure that they have all necessary expertise in the safety and regulatory ramifications of their applications. Customers acknowledge and agree that they are solely responsible for all legal. regulatory and safety-related requirements concerning their products and any use of WE products in such safety-critical applications. notwithstanding any applications-related information or support that may be provided by WE.

CUSTOMERS SHALL INDEMNIFY WE AGAINST ANY DAMAGES ARISING OUT OF THE USE OF WE PRODUCTS IN SUCH SAFETY-CRITICAL APPLICATIONS

USEFUL LINKS

Application Notes
www.we-online.com/appnotes

REDEXPERT Design Platform
www.we-online.com/redexpert

Toolbox
www.we-online.com/toolbox

Product Catalog
www.we-online.com/products

CONTACT INFORMATION

appnotes@we-online.com
Tel. +49 7942 945 - 0

Würth Elektronik eiSos GmbH & Co. KG
Max-Eyth-Str. 1 · 74638 Waldenburg
Germany
www.we-online.com